Hydrodynamic Behavior of Non-viscous Droplet Retraction in Leaking Faucets

Qige Wang, Xiaowei Shi, Manyu Zeng

November 1, 2024

Abstract

In this paper, we take a theoretical approach to analyze the dynamical behavior of water droplets from a leaking faucet. A steady-state approximation is used to describe the droplet formation process using the Young-Laplace equation. Then, the irregular detachment and propagation of the droplet are analyzed making use of the Navier-Stokes equation. Finally, we used COMSOL Multiphysics and completed a computer simulation on this problem by the Level Set Method.

Keywords: Young-Laplace Equation, Navier-Stokes Equation, Surface Tension

Contents

1 Introduction

When a water droplet is stuck to the end of a needle, it forms the shape of a half-oval. Such a shape is the result of a complex balance of gravitational force and surface tension, and it is a shape that has attracted mathematicians and physicists alike for several centuries.

In 1830, Gauss unified the work of Young and Laplace, deriving what is now known as the Young-Laplace equation. This equation describes a quantitative relationship between surface tension, interfacial pressure (Laplace pressure), and mean curvature of a liquid surface. Using this equation, it is possible to describe the stationary profiles of soap films and water droplets.

While the topic of fluid statics is now well-described using the Young-Laplace equation, the delicate nature of surface tension in fluid dynamics is still a subject of intense debate. By installing an iron mesh on a leaking faucet, it is possible to observe a periodic formation of water droplets on that mesh, initiating a series of rapidly deforming water drops.

Despite being a common phenomenon, such a setup poses a much greater challenge than a stationary pendant drop. Shi et. al. investigated leaking faucets using liquids with a viscosity much greater than that of water, leading to surprising results: the formation of drops was chaotic, the width of the droplet shrank to microscopic scales, the droplet's profile was non-smooth, and ripples oscillated across the surface (Constante-Amores, et. al.).

For several decades, further studies attempted to form quantitative approximations of the droplet's profile, but most theories failed to describe the phenomenon. The closest approximations were based on the interpolation of empirical evidence, and by combining existing models such as those used for modeling of elastic and hyperelastic deformations.

We took on this challenge after studying the Young-Laplace equation in preparation for the International Youth Physicists Tournament (IYPT). Although this was not a problem on the IYPT, we were deeply fascinated with the extreme phenomena occurring in thin liquid films. As a result, we pursued research on the formation of pendant drops, eventually evolving into this theoretical study on the dynamics of leaking faucets.

Considering that this area has been lacking in theoretical research, we've decided to conduct an investigation that's entirely theory-based. We attempted to model the formation of water droplets using a quasi-static approximation on a varied form of the Young-Laplace equation, from which we derive an equivalent

formulation of the surface energy reduction. Afterward, the sophisticated retraction and propagation of ripples are modeled in two stages using a combination of the Young-Laplace equation and the Navier-Stokes equation. This is then combined using a mollifier to combine the approximations for fluid break-up and the fully developed droplet profile. In the end, we attempted to solve these equations using Wolfram Mathematica and conducted experimental simulations using COMSOL Multiphysics.

2 Preliminary Experiment

In order to study this problem, we first observed the phenomenon by performing our preliminary experiment using faucets. We then made several basic assumptions based on the result of this preliminary experiment.

First, we used our school's water faucets to do the experiment. Initially, we found that the water flow out of the water pipe was unstable. We observed that the water didn't fill the entire cross-section of the water pipe, instead, it flowed along one side of the water pipe, and the spout then rotated around the tube. The angle of the water flow and the rotational direction were determined by micro-perturbation since it differed between every experiment, even those with the same initial conditions using the same faucet.

Observing other kinds of faucets in our school, homes, and online shops, we found that all the faucets have some kind of iron mesh on their outlets. Performing some experiments on these kinds of meshed faucets, we found that it has several properties that are very beneficial for our research:

- Water fills the pipe after passing the iron mesh.
- The flow after the iron mesh is laminar if the flow rate of water is sufficiently small, since both the velocity and the characteristic length of the flow decreases in the iron mesh.
- If the faucet faces vertically downwards after the iron mesh, it is rotationally symmetric about the central line of the water spout.
- The velocity distribution $\vec{v}(r)$ is more even after passing through the iron mesh and the radial component of the velocity is limited to a negligible order of magnitude compared to the axial component.

Figure 1: Household Faucet and Iron Mesh

According to these discoveries, we made some assumptions and approximations in our following analysis. After these analyses, we performed a preliminary experiment using household faucets

You can see the iron mesh very clearly on this picture.
Then we controlled the water faucet's flow rate and observed the shape and characteristics of the water under the faucet outlet.
We observed the formation of the water spout and water droplets under the faucet

Figure 2: Stable Water Spout

Figure 3: Formation of Water Droplet

Figure 4: Formation of Water Droplet

Figure 5: Formation of Water Droplet

Figure 6: Dropping of Water Droplet

3 Theoretical Analysis

3.1 Droplet Formation

3.1.1 Steady-State Profile

In this section, we discuss the droplet's profile until up to the detachment point. The droplet's profile at a certain point can be described in terms of its mean curvature $\frac{1}{R_1} + \frac{1}{R_2}$, and can be related to the Laplace pressure Δp at that point using the Young-Laplace equation:

$$\frac{\Delta p}{\gamma} = \frac{1}{R_1} + \frac{1}{R_2} \tag{1}$$

where $\gamma \approx 0.072\ \mathrm{Nm}^{-1}$ is the surface tension of water at room temperature. Let v be the velocity profile of the water and consider a cylindrical coordinate system (r, θ, z) with z-axis along the water droplet. We make the following assumptions:

- Inside the faucet and at the faucet-droplet interface, the flow is laminar. This is assumed because the pipe flow necessary for droplet formation has

low velocity, hence viscous shear forces dominate within the faucet.

- The flow is steady-state at the faucet-droplet interface, i.e., $\frac{\partial v}{\partial t} = 0$ at the end of the faucet. This is observed in experimental observations for low v, and is achievable through a steady water source.
- The cross-sectional flow is constant, i.e., $\frac{\partial v}{\partial \theta} = \frac{\partial v}{\partial r} = 0$. This is assumed due to the presence of an iron mesh at the end of the faucet, which acts as a stabilization device ensuring the symmetry of the flow.
- In cylindrical coordinates, the droplet's profile is axisymmetric about the z-axis. This is also based on observations of hanging water drops. Consequently, the droplet's profile can be uniquely described using a function $h(z)$, the droplet's cross-sectional radius at distance z from the faucet.

Now, we begin our analysis first with a stationary droplet in the presence of gravity. Define $h_z = \frac{\partial h}{\partial z}, h_{zz} = \frac{\partial^2 h}{\partial z^2}$. According to Pierre et. al., we can explicitly express the values of R_1 and R_2. We do this in the following manner:

$$\frac{\Delta p}{\gamma} = -\frac{h_{zz}}{(1+h_z^2)^{3/2}} + \frac{1}{h(1+h_z^2)^{1/2}} \tag{2}$$

In steady-state assumption, Δp gives the constant overpressure at a certain region in the droplet. The main contribution to this overpressure is the droplet's surface tension, and this surface tension balances with the gravitational pull to achieve a semi-stable profile. Assuming that the surface tension completely cancels out the weight of the water, we express Δp in terms of stagnation pressure

$$\frac{\rho g z}{\gamma} = -\frac{h_{zz}}{(1+h_z^2)^{3/2}} + \frac{1}{h(1+h_z^2)^{1/2}} \tag{3}$$

where ρ is the density of water and g is gravitational acceleration.

3.1.2 Dynamic Approximations

However, for an open faucet, it's obvious that the droplet's profile is not steady-state; the initial force balance is disturbed by net impulse of the faucet as well as changes in the droplet's volume.

To describe such scenarios, we discretize the time domain t and for each value of t, the droplet's profile can be described as an instantaneous balance of forces and viewed as steady-state. Since the deceleration of the fluid is not

known, we cannot directly compute the increase in Δp due to the impulse of the water flow; instead, we assume that the kinetic energy of the water flow is continuously and completely transformed into the overpressure of the drop.

We can view this change in overpressure equivalently as an infinitesimal fluctuation in surface tension, $\delta\gamma$, with the same unit as $\frac{d\gamma}{dt}$, $\mathrm{Nm^{-1}s^{-1}}$. In particular, this is equivalent to a uniform decrease in surface tension, since higher overpressure forces the surface area to increase against surface tension, and the magnitude of this change is proportional to the change in Δp. Let γ_E be a surface tension reduction term with a definition equation

$$\gamma_E = \int_0^T \delta\gamma \, dt$$

Assuming that the kinetic energy is uniformly distributed across the droplet's profile and making use of dimensional analysis, we have

$$\gamma_E = \min\left(\frac{\overline{E_K}t}{A}, k\right) + \overline{E_P} \tag{4}$$

where

$$\overline{E_K} = \frac{1}{2}\frac{dm}{dt}v^2 = \frac{1}{2}\rho\pi R^2 v^3$$

represents the kinetic energy distributed per unit time, and k is a term describing the maximum possible energy retention using a Hookean mass-spring model (Pierson et. al.), relating to the water flow rate and the elasticity of the droplet's surface (k is the fluid equivalent of the spring constant, and is to be determined experimentally). Now, we describe the distribution of excess weight using

$$\overline{E_P} = 2\pi\rho g \int_0^{Z(t)} \frac{hz}{c}\, dz - E_P' = \rho g \int_0^{Z(t)} z dz - E_P' = \frac{1}{2}\rho g Z^2(t) - E_P'$$

where $\overline{E_P}$ represents the excess gravitational potential energy per unit area that is converted into stagnation pressure. Moreover, E_P' is the gravitational potential energy per unit area in the equilibrium position corresponding to Equation 3; this is to ensure that fluid weight already accounted for in the equilibrium position 3 is not included again. Numerically, E_P' is equivalent to the value of $\overline{E_P}$ when $\overline{E_P} = \min\left(\frac{\overline{E_K}t}{A}, k\right)$. The other definitions are

1. $c(z,t)$ is the circumference of the water droplet with respect to the z-axis
2. $Z(t)$ is the minimum z-value for which $h(z) = 0 \ \ \forall z \geq Z(t)$

3. R is the radius of the column of water

4. A is the surface area of the droplet

5. m is the mass of water flowing from the faucet

Now, from Equations 3 and 4, we combine the surface tension term in the denominator with the surface tension reduction term:

$$\frac{\rho g z}{\gamma - \gamma_E} = -\frac{h_{zz}}{(1+h_z^2)^{3/2}} + \frac{1}{h(1+h_z^2)^{1/2}} \tag{5}$$

3.1.3 Boundary Conditions

To complete the analysis, we have the definition equation of A given by

$$A(t) = 2\pi \int_0^{Z(t)} h\,(z,t)\,\sqrt{1+h_z^2}\mathrm{d}z \tag{6}$$

Equations 4, 5, 6 solve for the three unknowns γ_E, h, A. To calculate the time-dependent constant $Z(t)$, we add the definition equation for volume:

$$V(t) = v\pi R^2 t = \pi \int_0^{Z(t)} h^2(z,t)\,dz \tag{7}$$

Combining Equations 4 to 7, we could theoretically evaluate this system of equations. As mentioned at the beginning, since there is no known analytical solution, we resolve the system in the following manner:

1. Determine the time t_0 at which the droplet reaches its detachment point (when surface tension doesn't support overpressure and droplet breaks).

2. Set the discrete time interval $\Delta t = \frac{t_0}{N}$, where N is the degree of precision.

3. For $k = 0, 1, ..., N$, set $t = k\Delta t$, set $Z(t)$ as an unknown constant, and solve Equations 4 to 7 for the steady-state droplet profile $h(z,t)$.

Finally, we can incorporate various boundary conditions, first by assuming that the droplet's profile evolves continuously and secondly by relying on experimen-

tal observations. Let $h_z = \frac{\partial h(z,t)}{\partial z}$, $h_{zz} = \frac{\partial h^2(z,t)}{\partial z^2}$, then

$$\begin{cases} Z(0) = 0 \\ h(0,t) = R \\ h_z(0,t) = 0 \\ h(Z(t),t) = 0 \\ h_z(Z(t),t) = -\infty \\ h_{zz}(Z(t),t) = -\infty \end{cases} \tag{8}$$

Let the "neck" of the droplet $z = n(t)$ be the location where

$$\begin{cases} h_{zz}(n(t),t) > 0 \\ h_z(n(t),t) = 0 \end{cases}$$

Notice that $n(t)$ is a local minimum of h, hence $\lim_{t\to t_0} n(t)$ is the z-coordinate of the detachment region. Since the neck drastically extends in length and a region $z = n(t) \pm \delta$ becomes very thin, immediately before detachment we have

$$\begin{cases} \lim_{t\to t_0} h(n(t),t) = 0 \\ \lim_{t\to t_0} h_z(n(t),t) = 0 \\ \lim_{t\to t_0} h_{zz}(n(t),t) = 0 \end{cases} \tag{9}$$

This allows us to explicitly characterize the droplet's dynamical behavior at time t_0. Applying this to Equation 5,

$$\lim_{t\to t_0} \frac{\rho g z}{\gamma - \gamma_E} = +\infty$$

from which

$$\lim_{t\to t_0} \gamma_E = \gamma \tag{10}$$

However, notice that Equation 5 is no longer applicable at t_0: this is because we have assumed that the kinetic energy due to incoming impulse is uniformly distributed, however, at t_0, the droplet is subdivided into 2 or more independent sections. Since these sections do not interact, the overpressure within each section is independent of each other, meaning that all our previous modeling fails. Modeling of detachment and later fluid retraction requires the use of a more general fluid equation such as the usage of the Navier-Stokes equations.

3.1.4 Approximation of $Z(t)$

Observing the Taylor expansion of h near $z = Z(t)$,

$$h(z) \approx \sum_{n=0}^{\infty} \frac{h^{(n)}(a)}{n!}(z-a)^n \approx h(Z(t)) + h'(Z(t))(z - Z(t)) \approx 0$$

Hence,

$$\lim_{z \to Z(t)} h'(z)(z - Z(t)) = 0$$

In particular, this suggests that

$$0 < \lim_{z \to Z(t)} h'(z) < \lim_{z \to Z(t)} \frac{1}{Z(t) - z}$$

Combined with semi-spherical approximation and experimental evidence suggesting $\lim_{z \to Z(t)} h'(z) = -\infty$, this leads to the crude approximation $h'(z) = -a(Z(t) - z)^{\alpha - 1}, h(z) = \frac{a}{\alpha}(Z(t) - z)^{\alpha}$ $(0 < \alpha < 1, a > 0)$.

Notice that

$$\lim_{z \to Z(t)} \frac{1}{h(1 + h_z^2)^{1/2}} - \frac{h_{zz}}{(1 + h_z^2)^{3/2}} = \lim_{z \to Z(t)} \frac{1}{h(1 + h_z^2)^{1/2}} = \frac{\rho g Z(t)}{\gamma - \gamma_E}$$

which is constant for specific t. Consequently, $\alpha = \frac{1}{2}$, and this allows us to determine a through graph-fitting, using the principle of least squares.

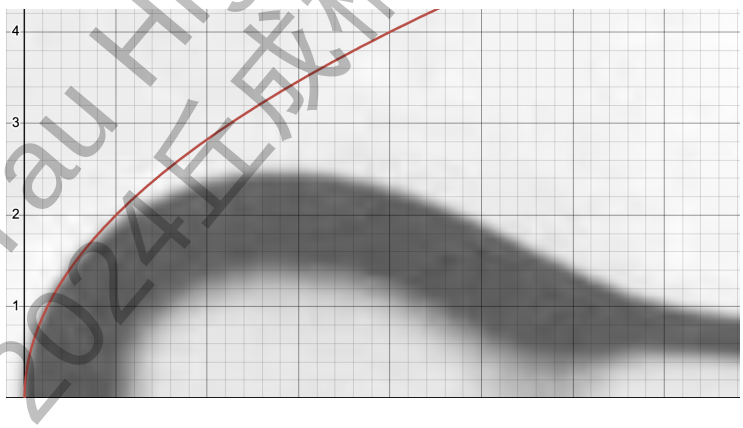

Figure 7: Curve-fitting using $a = 2, \alpha = \frac{1}{2}$

3.2 Droplet Retraction

In this section, we discuss the droplet's profile in a region near the breakup and in a region where the retraction is fully developed, using nondimensionalization methods. Then, we bridge the solutions to the two regions, ensuring that the two solutions overlap in some intermediate region, where the two expansions are both valid. We make 3 qualitatively physical assumptions:

- Near the breakup, surface tension, viscous force, and gravity are equally important.
- After the retraction is developed, the viscous force can be neglected, and surface tension and gravity are equally important.
- In a very small time and space, which is near the breakup and where the retraction is sufficiently developed, the system's behavior is invariant to scale, in other words, the system is self-similar (Gratton, J.).
- The transition behavior in the intermediate regime is smooth and monotonous.

The detailed justification is as follows:

- Near the breakup of a droplet, the fluid experiences extreme geometric and dynamic conditions: the droplet's neck becomes very thin, and forces that would typically be negligible in other parts of the droplet can no longer be ignored. This region is characterized by rapid changes in curvature, which amplify surface tension forces. Surface tension attempts to minimize the surface area by driving the liquid to contract. Simultaneously, the thinning neck results in a sharp increase in velocity gradients, which enhances viscous forces due to the high resistance to flow in confined spaces. Gravity, though generally weaker than surface tension in small droplets, still plays a role due to its contribution to the overall pressure distribution and its tendency to induce asymmetry in the droplet shape. In essence, near the singularity, no single force can be deemed dominant.
- The retraction and wave formation occur in the bulk of the droplet, where the flow is not significantly restricted by narrow channels or sharp edges that would otherwise create high-velocity gradients and increase viscous drag. After the breakup, as the lower part retracts and impacts the upper part, there are capillary waves on the lower surface of the droplet, driven by surface tension. On the other hand, gravity affects the capillary waves

by opposing the curvature-driven contraction and influencing the droplet's overall shape. Therefore, we assume that surface tension and gravity are equally important.

- In a very small time and space, the system's behavior is often self-similar because, near breakup or sharp retraction points, the system lacks a characteristic length or time scale that governs the dynamics. In these extreme conditions, the droplet's curvature, velocity, and other quantities become large and change rapidly, but they do so in a way that is geometrically and temporally proportional. As the droplet thins or retracts, the surface tension, inertia, and viscosity (though it is absent when the retraction is developed) balance each other in such a way that the system appears the same when rescaled in space and time. This scaling invariance means that, although the system evolves, the profile of the droplet and the flow field maintain a consistent shape, only shrinking or expanding as time progresses. The solutions depend on a single similarity variable, capturing both spatial and temporal evolution in a unified manner.

- Surface tension and gravity are the dominant forces in both the near-breakup and fully developed retraction stages, working together to maintain the droplet's cohesion and prevent rapid oscillations or unbounded changes in its profile. In the intermediate region, inertial effects help to smooth out the sharp gradients present near the breakup, allowing the droplet to transition into a thicker, rounded form without introducing abrupt variations. Additionally, because the model assumes no external perturbations, there is no external source of instability that could disrupt the smooth evolution of the droplet's shape and velocity fields. Experimental observations of droplet retraction also support this assumption, as they often reveal a continuous progression from the thin-necked breakup stage to a stable, thicker configuration.

3.2.1 Nondimensionalization of Navier-Stokes Equation

Navier-Stokes equation governs the behaviors of the droplet. As the droplet is axisymmetry, one can ignore the azimuthal components and write the Navier-Stokes equation as:

$$u_t + uu_r + vu_z = -\frac{1}{\rho}p_r + \nu(u_{rr} + \frac{1}{r}u_r + u_{zz} + \frac{1}{r^2}u) \tag{11}$$

$$v_t + uv_r + vv_z = -\frac{1}{\rho}p_z + \nu(v_{zz} + v_{rr} + \frac{1}{r}v_r) - g \tag{12}$$

and along with the continuity equation:

$$u_r + v_z + \frac{1}{r}u = 0 \tag{13}$$

where u is the radial velocity, and v is the axial velocity. We have the boundary conditions of balance of normal and tangential forces:

$$\begin{cases} n \cdot \sigma \cdot n = -\gamma(\frac{1}{R_1} + \frac{1}{R_2}) \\ n \cdot \sigma \cdot t = 0 \end{cases} \tag{14}$$

where n is the outward normal unit vector, t is the tangential unit vector, and σ is the stress tensor. From these boundary conditions, one can conclude

$$\frac{p}{\rho} - \frac{2\nu}{1+(h_z)^2}(u_r + v_z(h_z)^2 - (v_r + u_z)h_z) = \frac{\gamma}{\rho}(\frac{1}{R_1} + \frac{1}{R_2}) \tag{15}$$

from the fact that the sum of internal pressure, viscous contribution, and surface tension is zero at the surface, and

$$\frac{\nu}{1+(h_z)^2}(2u_r h_z + (v_r + u_z)(1-(h_z)^2) - 2v_z h_z) = 0 \tag{16}$$

from the fact that the sum of tangential forces is zero at the surface (Goldstein, S.).

In order to further simplify the equations, identify which factor is probably dominant, and make generalized conclusions, one needs to nondimensionalize the system. In this process, we introduce characteristic scales for all the elementary physical quantities such as length, time, and mass, then we represent all variables as ratios of the actual values to their characteristic scale. This makes all variables become dimensionless, but still describe the behavior of the system (Eggers, J.).

$$\begin{cases} r = r_0\tilde{r},\ z = z_0\tilde{z},\ t = t_0\tilde{t},\ m = m_0\tilde{m} \\ u = \frac{r_0}{t_0}\tilde{u},\ v = \frac{z_0}{t_0}\tilde{v},\ h = z_0\tilde{h},\ p = \frac{m_0}{z_0 t_0^2}\epsilon^n\tilde{p} \\ \rho = \frac{m_0}{z_0^3}\epsilon^n\tilde{\rho},\ \nu = \frac{z_0^2}{t_0}\epsilon^n\tilde{\nu},\ \gamma = \frac{m_0}{t_0^2}\epsilon^n\tilde{\gamma},\ g = \frac{z_0}{t_0^2}\epsilon^n\tilde{g} \end{cases} \tag{17}$$

Specifically, $r_0 = \epsilon z_0$, representing the thinness of the droplet. The magnitude

of ϵ characterizes the two extreme situations that we focus on in this section:

- When $\epsilon \ll 1$, it describes a situation where the droplet forms a thin jet before the breakup. The droplet's radius is much smaller than its length, and the fluid flow is primarily along the axial direction.
- When $\epsilon \gg 1$, it describes a situation where after the breakup, the retraction is substantially developed, and the droplet is thick. Accordingly, the radial dynamics dominate.

However, there are some physical quantities including length in their dimensions, and their definition indicates nothing between radial length and axial length, providing uncertainties in the nondimensionalization of these quantities. Therefore, exponents of ϵ should be included in their nondimensionalized expressions, and the power of ϵ will be settled later in the physical assumptions of the two regions.

3.2.2 Near the Breakup

Near the break-up of a droplet, the flow experiences extreme conditions: an infinitely thin neck, rapid changes in the velocity field, significant curvatures, and strong forces from surface tension and viscous stresses. At the point where the break-up actually happens, several physical quantities, like velocity, pressure, and curvature, become infinite or undefined. This is called a singularity.

Recalling our first assumption, by treating all three forces as equally significant, the assumption enables a thorough analysis of the near-breakup dynamics, capturing the rapid variations in physical properties like velocity and pressure. This balance facilitates the use of series expansions in small parameters such as the neck's thinness, helping isolate leading-order terms and reduce the radial dimension of the Navier-Stokes equations.

We firstly expand the $\tilde{u}$, $\tilde{v}$, and $\tilde{p}$ as a series in powers of ϵ (Eggers, J.).

$$\begin{cases} \tilde{v} = \Sigma_{i=0}^{\infty} \tilde{v}^{2j} (\epsilon \tilde{r})^{2j} \\ \tilde{u} = -\Sigma_{i=0}^{\infty} \frac{\tilde{v}_{\tilde{r}}^{2j}}{2j+2} (\epsilon \tilde{r})^{2j+1} \\ \tilde{p} = \Sigma_{i=0}^{\infty} \tilde{p}^{2j} (\epsilon \tilde{r})^{2j} \end{cases} \tag{18}$$

Now we want to insert the 18 into 11 and 12 and get the terms with the lowest

power of ϵ, thus we can reduce the Navier-Stokes equation to one-dimension.

$$\tilde{v}_{\tilde{t}}^0 + \tilde{v}^0\tilde{v}_{\tilde{z}}^0 = -\epsilon^n\frac{1}{\tilde{\rho}}\tilde{p}_{\tilde{z}}^0 + \epsilon^n\nu(4\tilde{v}^2 + \tilde{v}_{\tilde{z}\tilde{z}}^0) - \epsilon^n\tilde{g} \tag{19}$$

Next, the pressure is related to surface tension and curvature. From 16 and 17, and notice that $R_1 = h$ and $\frac{1}{R_2} \approx 0$ we have:

$$\begin{cases} \epsilon^n\tilde{p}_{\tilde{z}}^0 = \epsilon^n\tilde{\gamma}(\frac{1}{\tilde{h}})_{\tilde{z}} \\ -\tilde{v}^0\tilde{h}_{\tilde{z}} + 2\tilde{v}^2 - \frac{1}{2}\tilde{v}_{\tilde{z}\tilde{z}}^0\tilde{h} - 2\tilde{v}_{\tilde{z}}^0\tilde{h}_{\tilde{z}} = 0 \end{cases} \tag{20}$$

Incorporate 19 and 20, and according to our assumption, all forces are equally important, so the resultant powers of ϵ of every term should be zero. Now we have our final nondimensionalized expression of the Navier-Stokes equation:

$$\tilde{v}_{\tilde{t}}^0 + \tilde{v}^0\tilde{v}_{\tilde{z}}^0 = -\frac{\tilde{\gamma}}{\tilde{\rho}}(\frac{1}{\tilde{h}})_{\tilde{z}} + 3\tilde{\nu}\frac{1}{\tilde{h}^2}(\tilde{v}_{\tilde{z}}^0\tilde{h}^2)_{\tilde{z}} + \tilde{g} \tag{21}$$

and the nondimensionalized continuous equation:

$$\tilde{h}_{\tilde{t}} + \tilde{v}^0 + \frac{\tilde{h}}{2}\tilde{v}_{\tilde{z}}^0 = 0 \tag{22}$$

3.2.3 After the Retraction Is Developed

Recalling our second assumption, viscosity is neglected, and surface tension and gravity are equally important. By assuming that only surface tension and gravity are significant, this approach isolates the primary forces shaping the retraction dynamics and capillary wave patterns, capturing the droplet's evolution in its stable retraction phase. Consequently, the mathematical treatment becomes more tractable, enabling analytical or semi-analytical solutions that describe the dominant shape characteristics in this regime.

We still start with expanding the fields as a series in powers of ϵ but with respect to the axial variable.

$$\begin{cases} \tilde{u} = \Sigma_{i=0}^{\infty}\tilde{u}^{2j}(\frac{\tilde{z}}{\epsilon})^{2j} \\ \tilde{v} = -\Sigma_{i=0}^{\infty}\frac{\tilde{u}_{\tilde{z}}^{2j}}{2i+2}(\frac{\tilde{z}}{\epsilon})^{2i+1} \\ \tilde{p} = \Sigma_{i=0}^{\infty}\tilde{p}^{2j}(\frac{\tilde{z}}{\epsilon})^{2j} \end{cases} \tag{23}$$

Notice that here we want the terms with the highest power of ϵ since now

$\epsilon \gg 1$. Similarly, additionally known 2, one can get the final nondimensionalized expression of the Navier-Stokes equation here:

$$\tilde{u}^0_{\tilde{t}} + \tilde{u}^0\tilde{u}^0_{\tilde{r}} = -\frac{1}{\tilde{\rho}}\tilde{\gamma}(\frac{1}{\tilde{h}(1+(\tilde{h}_{\tilde{z}})^2)^{\frac{1}{2}}} - \frac{\tilde{h}_{\tilde{z}\tilde{z}}}{(1+(\tilde{h}_{\tilde{z}})^2)^{\frac{3}{2}}})_{\tilde{r}} - \tilde{g} \tag{24}$$

and corresponding continuous equation:

$$\tilde{h}_{\tilde{t}} - \frac{\tilde{z}}{2\epsilon}\tilde{u}^0_{\tilde{z}}\tilde{h}_{\tilde{z}} - \tilde{u}^0 = 0 \tag{25}$$

3.2.4 Mollifying the Solutions

In the previous two sections, we separately derived the Navier-Stokes equation for the region near the breakup and after the retraction is fully developed. In this section, our goal is to find a method to approximate the system's global behavior.

With our self-similar assumption, we can transform a set of PDEs (which is very complex) into ODEs using similarity variables. Therefore, we can bridge between the region near the breakup and the region where the retraction is substantially developed, as the 2 sets of ODEs are in the same space. Finally, we use the mollification technique to connect the solutions.

On the other hand, our last assumption states that physical properties like velocity, pressure, and height do not experience abrupt oscillations or discontinuities, ensuring that the solution can smoothly interpolate between the two regimes. By assuming bounded behavior in the intermediate region, the mollifier effectively serves as an "averaging" function that unifies the two extreme states, forming a global, continuous, and physically realistic solution.

The first step here is to redefine the elementary physical quantities. We still use the same sign but different definitions to prevent further confusion. We want to find a combination of the inherent quantities to form a quantity with dimensions $[L]$ and $[T]$. The characteristic length is defined as $x_e := \mu^{\frac{2}{3}}\rho^{\frac{1}{3}}\gamma^{-\frac{1}{3}}$, and the characteristic time is defined as $t_e = \nu^{\frac{1}{3}}\rho^{\frac{2}{3}}\gamma^{-\frac{2}{3}}$. We simply let $r_0 = z_0 = x_e$ and $t_0 = t_e$.

Now we assume the variable of 21 and 22 to be $\iota = \frac{\tilde{z}}{\tilde{t}^\alpha}$ and the variable of 24 and 25 to be $\zeta = \frac{\tilde{r}}{\tilde{t}^\beta}$. Next, we expect self-similar solutions for both $\tilde{h}$ and

velocity in both regimes, which are defined as:

$$\begin{cases} \tilde{v}^0(\tilde{z},\tilde{t}) = \tilde{t}^{a_1} f_1(\iota) \\ \tilde{h}(\tilde{z},\tilde{t}) = \tilde{t}^{b_1} g_1(\iota) \end{cases} \tag{26}$$

for regions near breakup, and

$$\begin{cases} \tilde{u}^0(\tilde{r},\tilde{t}) = \tilde{t}^{a_2} f_2(\zeta) \\ \tilde{h}(\tilde{r},\tilde{t}) = \tilde{t}^{b_2} g_2(\zeta) \end{cases} \tag{27}$$

for the region after the retraction is developed.

All the exponents here α, β, $a_{1,2}$, and $b_{1,2}$ can be determined using dimensional analysis, $\alpha = \beta = \frac{1}{2}$ $a_1 = a_2 = 1$, and $b_1 = b_2 = -\frac{1}{2}$. Now one can apply the chain rule many times to replace the partial derivatives in governing equations 21, 22, 24, and 25 with ordinary derivatives of self-similar variables. The resultant ODEs are:

$$\begin{cases} f_1 + \iota f_1' + f_1 f_1' = -\frac{\tilde{\gamma}}{\tilde{\rho}} (\frac{1}{g_1})' + 3\tilde{\nu}(f_1' g_1^2)' - \tilde{g} \\ -\frac{1}{2} g_1 + \iota g_1' + f_1 + \frac{1}{2} g_1 f_1' = 0 \end{cases} \tag{28}$$

near the breakup, and

$$\begin{cases} f_2 + \zeta f_2' + f_2 f_2' = \tilde{\gamma} \left(\frac{1}{t^{-\frac{1}{2}} g_2(\zeta) \left(1 + t^{-2} (g_2'(\zeta))^2\right)^{1/2}} \frac{t^{-\frac{3}{2}} g_2''(\zeta)}{\left(1 + t^{-2} (g_2'(\zeta))^2\right)^{3/2}} \right) - \tilde{g} \\ -\frac{1}{2} g_2 + \zeta g_2' + f_2 + \frac{1}{2} g_2 f_2' = 0 \end{cases} \tag{29}$$

after the retraction is developed.

By incorporating boundary conditions, one can solve for $f_{1,2}$ and $g_{1,2}$. However, they are only valid in different regions. Now we want to ensure that the solutions from each regime overlap in an intermediate region. This allows us to transition smoothly between the two regimes, creating a unified solution for the droplet retraction process. We introduce mollifier, a mathematical technique that is employed to "smooth" or "regularize" functions or distributions that may not be differentiable or continuous. Here are some good properties of a mollifier $\phi(x)$ ($x \in \mathbb{R}^n$):

1. A mollifier is an infinitely differentiable (smooth) function.

2. It typically has compact support, meaning it is non-zero only within a

finite region of space.

3. The mollifier is non-negative everywhere.

4. The integral of a mollifier over its entire domain is 1, ensuring that it preserves the overall magnitude of a function when applied.

A standard mollifier is defined as:

$$\phi(x) = \begin{cases} Ce^{\frac{1}{|x|^2-1}}, \text{ if} |x| < 1 \\ 0, \text{ else} \end{cases} \tag{30}$$

where C is a constant ensures normalization, but for this application, we can ignore normalization since we only need a smooth connection between the two solutions.

Mollifiers are used to approximate non-smooth or discontinuous functions with smooth functions. In other words, we can get a smooth function connecting the middle area between the two regions, and is also valid in the two extreme regions. The final global expressions for any values of ϵ of velocity and height are (to avoid misconception, we use $\tilde{w}$ to represent velocity):

$$\begin{cases} \tilde{w} = \phi(\epsilon)\tilde{t}f_1(\iota) + (1-\phi(\epsilon))\tilde{t}f_2(\zeta) \\ \tilde{h} = \phi(\epsilon)\tilde{t}^{-\frac{1}{2}}g_1(\iota) + (1-\phi(\epsilon))\tilde{t}^{-\frac{1}{2}}g_2(\zeta) \end{cases} \tag{31}$$

By using a mollifier, we smoothly connect the self-similar solutions for both the velocity and the height. This approach ensures a continuous and smooth transition between the near-breakup and fully developed retraction regimes, allowing for a unified description of the droplet retraction process across the entire time and space scales.

4 Computer Simulation

After theoretical Analysis, we used the computer software "COMSOL Multiphysics" to simulate the physics process.

According to our assumption, we used the multi-phase flow and laminar flow physics field in COMSOL Multiphysics.

We proved that the assumption of no radial velocity gradient is correct by getting the velocity distribution at the outlet of the faucet in simulation and found that the function (normalized) is like

This shows that the approximation won't affect the result much.

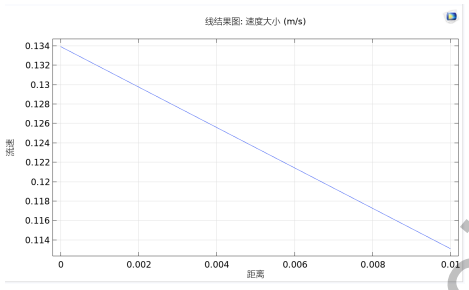

Figure 8: Proof of Assumption

We first decided to use the dynamic mesh method to simulate the motion of the liquid. However, we didn't find any water droplets separating out from the water spout no matter how small the flowing rate is and the software raises errors frequently. After reading some instructions on COMSOL's official website, we realized that the dynamic mesh method of simulation is not effective when the topology of the fluids changes (we'll explain this further). Then we used the level-set method in the simulation.

4.1 Level-Set Method

The level-set method in computational fluid mechanics is an effective method when dealing with multi-phase flow. It can deal with complex topological changes on the water-air surface. For example

- Air comes into the water forming a bubble
- Water goes into the air forming water droplets
- Bubbles and water droplets merge or decompose
- Bubbles and water droplets touch the major boundaries again

This method uses a phase function $\phi(\vec{r})$ taking a point in the space $\vec{r}$ for input and output 1 if this point is occupied by water and 0 otherwise. The computer, of course, cannot deal with water-air boundaries since the function jumps from 0 to 1 sharply at this boundary, but COMSOL can solve this by blurring the boundary into a continuous function. The density and other features of the fluids change linearly on the border. Take density as an example, the density is

given by

$$\rho\left(\vec{r}\right) = \rho_{\text{air}} + \phi\left(\vec{r}\right)\left(\rho_{\text{water}} - \rho_{\text{air}}\right) \tag{32}$$

We chose the wet-wall boundary condition in the simulation and solved the problem according to the Navier-Stokes Equation under laminar flow conditions.

4.2 Velocity Results

The graph of resultant velocity is shown below, we took the image at time $t = 0, 0.3, 0.5, 1.0$s and drew both the magnitude of the velocity and the flow line to indicate the direction of the flow.

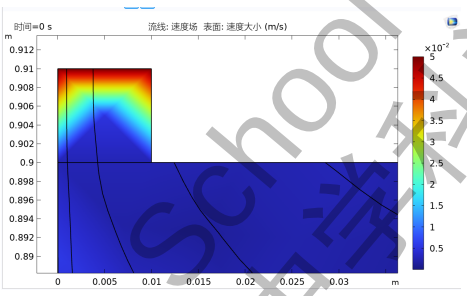

Figure 9: Velocity at $t = 0$s

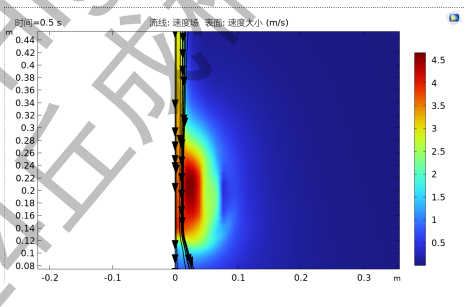

Figure 10: Velocity at $t = 0.3$s

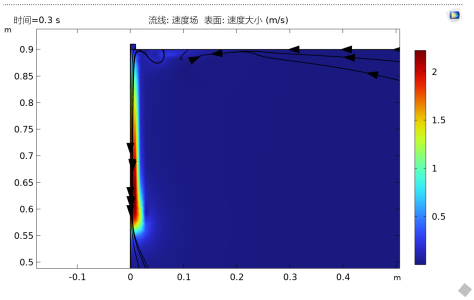

Figure 11: Velocity at $t = 0.5$s

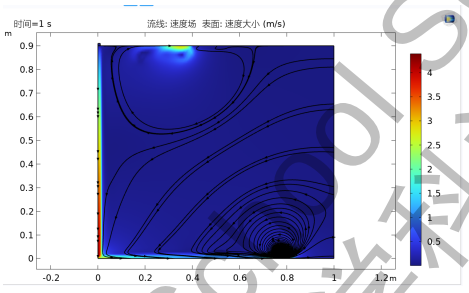

Figure 12: Velocity at $t = 1$s

4.3 Phase Change Boundaries

Since the function $\phi(\vec{r})$ is continuous and varies from 0 to 1 continuously, we cannot determine the boundary precisely. If the boundary thickness variable is set to a small value, we need more mesh to ensure the solution of dependent variable functions converges, meaning an enormous amount of time is required for the software to give results. Hence we used the boundary thickness 2mm and got the possible distribution of the result as below (the colored region). We took the time $t = 0, 0.2, 0.4, 0.9$s

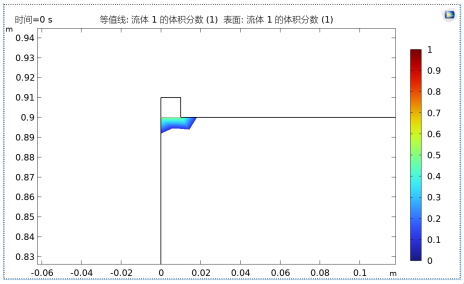

Figure 13: Phase Distribution at $t = 0$s

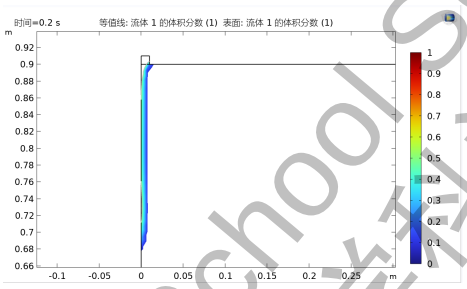

Figure 14: Phase Distribution at $t = 0.2$s

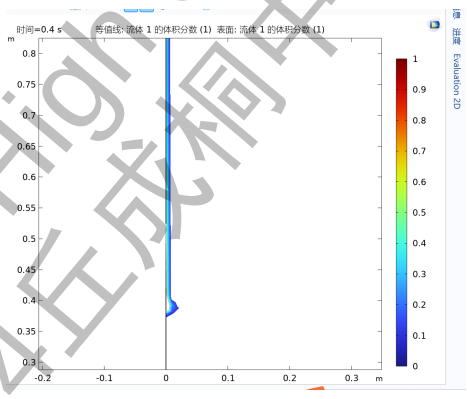

Figure 15: Phase Distribution at $t = 0.4$s

5 Conclusion

In this paper, we established a quantitative approximation of the dynamic profile of a water droplet suspended from a leaking faucet. We started off with a preliminary experiment to determine the overall profile of the droplet and used these results to develop the necessary assumptions for our fluid approximations.

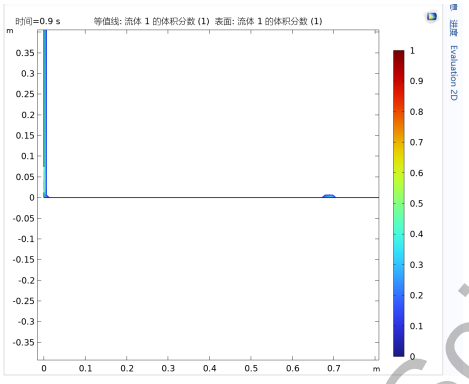

Figure 16: Phase Distribution at $t = 0.9$s

Afterward, we analyzed the profile of the water droplet separately for the formation, detachment, and retraction stages.

There are two novel theoretical aspects of our paper that, to the authors' extent of knowledge, have not been used before. First of all, we used the Young-Laplace equation to describe the formation of the droplet, while most previous papers have used advanced partial differential equations such as the Navier-Stokes equation. Secondly, we have formulated an approximate solution to the retraction phase using a system of differential equations, while previous papers usually used larger systems of partial differential equations. Thus, we made an effort to simplify the theoretical aspects of both the formation and detachment of the droplet.

While we have made some progress towards a new quantitative approach, our research is still lacking in many aspects. Although the equations have been largely simplified through fluid approximations, they're still too sophisticated to be fully resolved analytically or using Mathematica. Furthermore, both parts of the theory made use of extreme approximations, and their induced margin of error has not been assessed. In future work, we will try to improve the fluid approximations, particularly in calculating the mollifier and the reduction in surface tension. We will also conduct a bifurcation analysis to determine the behavior of possible analytical solutions at extreme values.

References

[1] Constante-Amores, C. R., Assen Batchvarov, Lyes Kahouadji, Shin, S., Jalel Chergui, Damir Jurić, and Matar, O. (2021). Role of surfactant-induced Marangoni stresses in drop-interface coalescence. Journal of Fluid Mechanics, 925. https://doi.org/10.1017/jfm.2021.682

[2] Eggers, J. (1995). Theory of drop formation. Physics of Fluids, 7(5), 941–953. https://doi.org/10.1063/1.868570

[3] Goldstein, S. (1933). 1. Hydrodynamics. By Sir Horace Lamb. Sixth Edition. Pp. xv, 738. 45s. 1932. (Cambridge University Press) - 2. Einführing in die Theorie der zähen Flüssigkeiten. By W. Müller. Pp. x, 367. Rm. 22.80. 1932 (Akademische Verlagsgesellschaft, Leipzig). The Mathematical Gazette, 17(224), 215–217. https://doi.org/10.2307/3607627

[4] Pierson, J.-L., Magnaudet, J., Edson José Soares, and Stéphane Popinet. (2020). Revisiting the Taylor-Culick approximation: Retraction of an axisymmetric filament. Physical Review Fluids, 5(7). https://doi.org/10.1103/physrevfluids.5.073602

[5] Shi, X., Brenner, M., and Nagel, S. R. (1994). A Cascade of Structure in a Drop Falling from a Faucet. Science, 265(5169), 219–222. https://doi.org/10.1126/science.265.5169.219

[6] Widom, B. (2004). Capillarity and Wetting Phenomena: Drops, Bubbles, Pearls, Waves Capillarity and Wetting Phenomena: Drops, Bubbles, Pearls, Waves, Pierre-Gilles de Gennes , Françoise Brochard-Wyart , and David Quéré (translated from French by Axel Reisinger) Springer-Verlag, New York, 2004. ISBN 0-387-00592-7. Physics Today, 57(12), 66–67. https://doi.org/10.1063/1.1878340

[7] Zhang, D. F., and Stone, H. A. (1997). Drop formation in viscous flows at a vertical capillary tube. Physics of Fluids, 9(8), 2234–2242. https://doi.org/10.1063/1.869346

[8] Gratton, J. (1991). Similarity and self similarity in fluid dynamics. New York: Gordon And Breach Science Publishers.